Contents lists available at ScienceDirect

Biosensors and Bioelectronics

journal homepage: http://ees.elsevier.com

Influence of molecular size and zeta potential in electrokinetic biosensing

Siddharth Sourabh Sahu [a], Christiane Stiller [b], Sara Cavallaro [c], Amelie Eriksson Karlström [b], Jan Linnros [c], Apurba Dev [a,*]

[a] Division of Solid State Electronics, Department of Engineering Sciences, The Angstrom Laboratory, Uppsala University, Uppsala, Sweden
[b] Department of Protein Science, School of Chemistry, Biotechnology, and Health (CBH), KTH Royal Institute of Technology, Stockholm, Sweden
[c] Department of Applied Physics, School of Engineering Sciences, KTH Royal Institute of Technology, Kista, Sweden

ARTICLE INFO

Keywords
Biosensor
Electrokinetics
Streaming current
Zeta potential
Influence of molecular size and charge
Improved sensitivity

ABSTRACT

Electrokinetic principles such as streaming current and streaming potential are extensively used for surface characterization. Recently, they have also been used in biosensors, resulting in enhanced sensitivity and simpler device architecture. Theoretical models regarding streaming current/potential studies of particle-covered surfaces have identified features such as the particle size, shape and surface charge to influence the electrokinetic signals and consequently, the sensitivity and effective operational regime of the biosensor. By using a set of well-characterized proteins with varying size and net surface charge, this article experimentally verifies the theoretical predictions about their influence on the sensor signal. Increasing protein size was shown to enhance the signal when their net surface charge was either opposite to that of the sensor surface, or close to zero, in agreement with the theoretical predictions. However, the effect gradually saturates as the protein size exceeds the coulomb screening length of the electrolyte. In contrast, the proteins containing the same type of charge as the surface show little or no difference, except that the signal inverts. The magnitude of the surface charge was also shown to influence the signal. The sensitivity of the technique for protein detection varied over two orders of magnitude, depending upon the size and surface charge. Furthermore, the capacity of the electrokinetic method for direct electrical detection of various proteins, including those carrying little or no net electric charges, is demonstrated.

1. Introduction

The demand for sensitive, portable and inexpensive devices has motivated an explosive growth in the field of electronic biosensors during the past several decades (Chen et al., 2010, 2017). The continuously increasing repertoire of potential biomarkers contains a variety of targets, which have a range of different physical properties. For example, the size of a targeted marker may vary over a large range: from relatively small molecules like metabolites and peptides, nucleic acids and proteins to large particles like microvesicles and cells. Due to the presence of various functional groups, the biomarkers also possess widely varying electric charges, usually quantified in terms of their zeta potential. Clearly, depending on the sensing modalities, these physical properties are expected to influence the performance of a sensor to various degrees. Therefore, it is necessary that these effects are properly investigated and taken into consideration while benchmarking the performance of a sensor.

In the context of electrokinetic sensors (Dev et al., 2016), where an adsorbed particle perturbs both the local hydrodynamics and electrostatics (Joly et al., 2004), the influence of physical properties like the size and charge of the adsorbed particle is a particularly important consideration. The electrokinetic principles such as streaming current and streaming potential have been widely explored for precise determination of surface coverage and deposition kinetics of various organic/inorganic particles (Downs et al., 2019; Hanaor et al., 2014) as well as biological molecules/particles such as antibodies (Dev et al., 2016), DNA (Li et al., 2018) and extracellular vesicles (Cavallaro et al., 2019). The streaming current (I_S), or the streaming potential (V_S), is generated when an electrolyte is forced to flow through a channel under an applied pressure. It is one of the many electrokinetic phenomena that owe their existence to the electrical double layer (EDL) (Delgado et al., 2007; Joly et al., 2004) occurring at the solid-liquid interface. The generated I_s is proportional to the applied pressure and it is related to the surface zeta potential (ζ) by the following relation:

$$\zeta = \frac{\Delta I_S}{\Delta P}\frac{\eta}{\varepsilon_r \varepsilon_0}\frac{L}{A} \tag{1}$$

which holds for a cylindrical channel. Here η is the dynamic viscosity of the liquid, $\varepsilon_r\varepsilon_0$ is the electrical permittivity, $\frac{\Delta I_S}{\Delta P}$ is the slope of the streaming current vs. pressure graph, while L **and** A are the length and area of cross section of the channel. ζ is a useful quantity in the con-

* Corresponding author.
E-mail address: apurba.dev@angstrom.uu.se (A. Dev)

https://doi.org/10.1016/j.bios.2020.112005
Received 12 October 2019; Received in revised form 26 December 2019; Accepted 3 January 2020
Available online xxx
0956-5663/

text of electrical surface characterization, and can be used to compare different charged surfaces regardless of the pressure and flow profiles, or the electrolyte used for measurement.

The influence of structural and electrostatic attributes of adsorbed particles on the electrokinetic phenomena has also been well investigated by theoretical methods (Delgado et al., 2007). These investigations were mainly driven by the Hayes group (Hayes, 1999; Hayes et al., 1999) and the Adamczyk group (Adamczyk et al., 2010; Sadlej et al., 2009; Zembala et al., 2001; Zembala and Adamczyk, 2000). The derivation of equation (1) involves solving the Navier-Stokes and Poisson-Boltzmann equations (Adamczyk et al., 2010). However, in the presence of surface-attached particles, these equations become considerably complex to solve analytically. The Adamczyk model hence adopts a numerical approach to tackle the problem (Sadlej et al., 2009). The resulting solution expresses the modified streaming current, I_s in terms of the surface coverage by the bound particles, θ, and is given by:

$$I_s = I_{s0}\left[1 - A_i\theta + \frac{\zeta_p}{\zeta_i}A_p\theta\right] \quad (2)$$

where A_i and A_p are given by, $A_i = \frac{1-e^{-C_i\theta}}{\theta}$ and $A_p = \frac{1-e^{-C_p\theta}}{\theta}$. ζ_i is the zeta potential of the channel surface before any particle is adsorbed and ζ_p is the zeta potential of the particles. The parameters C_i and C_p represent the changes in the macroscopic flow and electrical charge density fluctuations, respectively, induced by the adsorbing particles on the interface (Adamczyk et al., 2010). They are dimensionless functions of the parameter a/λ, where a is the radius of the particle and λ is the Debye screening length. The dependence of C_i and C_p on a/λ has been calculated numerically by solving the Poisson-Boltzmann and Navier-Stokes equations (Sadlej et al., 2009; Zembala and Adamczyk, 2000).

Various experimental attempts to investigate the validity of the above theoretical predictions only concern large particles, in the regime where a>100nm (Michelmore and Hayes, 2000; Zembala and Adamczyk, 2000). However, in the context of biomolecule detection, the size range in the order of $a \sim 1$ nm is also significant, given that a large number of biomolecules of diagnostic importance lie in this regime. In addition, the effect arising from the molecular charge has not been adequately addressed in the literature. Therefore, this article attempts to investigate the influence of two important physical features of a biological molecule/particle i.e., size and charge, on an electrokinetic sensor that utilizes the streaming current technique for measurements. Experimental investigations were performed by using a set of well characterized protein molecules having their size in the range of 9–460 kDa (~1–5 nm radius), which is in the order of the λ (=2.3 nm, see the supplementary information for its estimation) of the electrolyte used for the experiments. The results, further simulated by using the theoretical model developed by Adamczyk and co-workers (Adamczyk et al., 2010), show good qualitative agreement with the theoretical predictions and clearly demonstrate that the sensor response is strongly influenced by both the size and the zeta potential of an adsorbed protein. In terms of charge, the response is stronger when the particles and the sensor surface bear opposite types of charge, and weaker when both bear the same type of charge. The response was also found to increase with size in the case of charge neutral molecules as well as for those containing opposite charge. Further, the sensitivity of the technique was shown to vary over two orders of magnitude depending upon the size and charge parameters of the protein studied.

2. Materials

Ultra-pure water was produced using the Milli-Q synthesis water purification system (Merck Millipore, Germany). Phosphate buffered saline solution (1x PBS) composed of 137 mM NaCl, 2.7 mM KCl and 10 mM phosphate buffer with a pH of 7.4 was obtained from VWR. Micro-capillaries made of silica, and with a diameter of 25 μm were obtained from Swedish Acreo. All other chemicals were purchased from Sigma-Aldrich unless stated otherwise.

3. Methods

3.1. Preparation of proteins

As initial test proteins, a class of antibody-mimetics called affibodies was used. These were derived from the 7 kDa B-domain of staphylococcal protein A and differ by 13 amino acids in the target-specific binding surface (Löfblom et al., 2010). All affibody domains used in this study are based on the same rod-shaped three-helix-bundle structure (Tashiro et al., 1997), whilst having different amino acid compositions in two of the helices (table SI). The affibodies were produced in monomeric and dimeric format. Dimeric affibodies were produced as head-to-tail fusion proteins linked with a S_4G sequence. All constructs carried a C-terminal cysteine, Sortase A recognition motif and H_6-tag. Formation of intermolecular disulfide bonds was prevented through alkylation of the proteins with iodoacetamide and the success of labelling was analysed via analytical size exclusion chromatography (SEC). Further details on affibody expression, purification and alkylation are stated in the supplementary data. As representatives of proteins with higher molecular weight, the monoclonal antibody Cetuximab (Erbitux infusion solution, 5 mg/mL from Merck Serono) and the complement component C1Q (Sigma; C1740) were utilized.

The dimensions of the monomeric and dimeric affibodies we chose are of the order of λ, making them suitable to test the performance of our device at this length-scale. Most proteins fold into globules by the formation of a hydrophobic core from nonpolar amino acids (Erickson, 2009). This allows us to approximate all the proteins used in this study to be spherical for the sake of simplicity, even though they are not strictly so. We measured their apparent molecular weights via size exclusion chromatography (SEC) and then calculated their apparent hydrodynamic radii. The surface zeta potential of all proteins is measured via electrophoretic scattering (ELS) (Table 1). The details of both analytical methods are provided in the supplementary information. The final size and charge parameters of the various proteins used are given in Table 1.

3.2. Capillary functionalization

The inner surface of the capillaries was functionalised using the protocol outlined in our earlier work (Dev et al., 2016). The surface was first cleaned with a 5:1:1 solution of Milli-Q water, 30% H_2O_2 and 25% NH_4OH at 88 °C for 10 min. This process also activates the hydroxyl group for silanisation carried out in the next step, with 5% w/v APTES in 95% ethanol. This was followed by incubation of 1% glutaraldehyde (GA) solution for 1 h. The electrical measurements were carried out directly afterwards. For control experiments, the GA surface was deactivated by flowing Tris-ethanolamine (0.1 M Tris buffer and 50 mM ethanolamine, pH 9.0) blocking solution for 30 min, followed by 0.05% casein solution for 30 min before starting the measurements. Prior to the experiments, inner walls of all connecting tubes and the hollow Pt electrode were also treated with 0.05% casein for 30 min to minimize their contribution to the signal. The length of the capillaries used in the experiments was ~4.5 cm.

3.3. Fluidic and electrical measurements

A schematic of the experimental setup is shown in our previous work (Cavallaro et al., 2019). Briefly, a commercial pressure regulator from Elveflow (OB1) was utilized for generating the pressure driven flow through a micro-capillary. The pressure was made to alternate between 1.5 and 3 bar so as to form a continuous train of rectangular pulses. The flow rate in response to the applied pressure was further monitored via a flow sensor (Elveflow, MSF3). The pressure pulses produced analogous pulses in the streaming current, as expected

Table 1
Size and charge information for investigated proteins: apparent molecular weights as measured with SEC, hydrodynamic radii derived and surface zeta potential (ζ_p) measured via ELS (for details see supplementary information).

Protein	Construct	Symbol	Apparent molecular weight (kDa)	Hydrodynamic radius (nm)	Normalized radius, a_r	ζ_p (mV)
anti-HER3	Monomer	S1A	10.6 ± 0.1	1.5	0.62	−1.9 ± 0.3
anti-EGFR	Dimer	S2A	21.7 ± 0.6	2.0	0.87	−7.5 ± 0.9
anti-EB3	Monomer	S1B	11.1 ± 0.3	1.5	0.63	−8.7 ± 0.6
anti-EB3	Dimer	S2B	25.9 ± 0.1	2.2	0.92	−9.2 ± 0.7
anti-HER2	Monomer	N1	7.3 ± 0.3	1.3	0.55	0.2 ± 0.1
anti-HER3	Dimer	N2	18.9 ± 0.4	1.9	0.83	0.3± 0.2
anti-HER2	Dimer	O2	14.0 ± 0.6	1.8	0.75	2.7 ± 0.3
Cetuximab	–	CET	193.4 ± 2.6	3.8	1.63	1.5 ± 0.5
C1Q	–	C1Q	460 [a]	5.1	2.18	19.6 ± 0.3

[a] This value has been obtained from literature (Horak et al., 2018).

from equation (1). The streaming current measurements were carried out via a hollow Pt tube electrode at the inlet and an Ag/AgCl reference electrode at the outlet, which were connected to a highly sensitive source meter (Keithley 2636A). Using the current and the pressure data, the zeta potential of the surface as a function of time was derived by utilizing equation (1). However, equation (1) assumes an arbitrarily smooth surface, along with uniformity both in the charge distribution on the capillary surface and velocity profile of the liquid along the flow direction (Levine et al., 1975), all of which are violated when a protein attaches to the surface. Hence, the data presented in this article is represented in terms of apparent zeta potential (ζ^*). The ζ^* of the surface was measured by flowing 0.1× PBS buffer, hereafter referred to as baseline measurements, before and after the injection of sample plug containing various proteins. Unless otherwise stated, a fixed concentration of 100 nM and a 40 min injection of sample plug was maintained for all the proteins in order to obtain a comparable surface coverage. The net signal, i.e. the difference between the initial (ζ_i^*) and final (ζ_f^*) zeta potential for the two baselines ($\mathbf{\Delta}\zeta^* = \zeta_f^* - \zeta_i^*$) is considered for all the analysis presented here. It should be noted that when $\mathbf{\Delta}\zeta^*>0$, we have $|\zeta_f^*| < |\zeta_i^*|$ and vice versa.

4. Results

To understand the expected behaviour of $\mathbf{\Delta}\zeta^*$ upon surface adsorption of the investigated proteins, we first carried out simulations based on the Adamczyk model (Adamczyk et al., 2010; Zembala et al., 2003). For this, we first noted that our experiments involve applying a pressure pulse alternating between two fixed values and recording the difference in the corresponding streaming current values, δI_s. Note that this requires I_s vs. P curve to be linear, which is indeed the case, as shown in the supplementary information (see figure S1). Hence, we can rewrite equation (2) as:

$$\delta I_s = \delta I_{s0}\left[1 - A_i\theta + \frac{\zeta_p}{\zeta_i}A_p\theta\right] \tag{3}$$

It is useful to express equation (3) in terms of the zeta potential, so as to normalize over the different structural (channel dimensions) and material parameters. Again, we emphasize here that we are referring to the apparent zeta potential and not the actual surface zeta potential. Using the expression in equation (1), we get,

$$\zeta_f^* = \zeta_i^*\left[1 - A_i\theta + \frac{\zeta_p}{\zeta_i}A_p\theta\right] \tag{4}$$

Equation (4) is valid for the entire range of surface coverage practically achievable through experiments (Adamczyk et al., 2010). Upon substituting the expressions of A_i and A_p mentioned earlier, we finally arrive at:

$$\begin{aligned}\Delta\zeta^* &= \zeta_f^* - \zeta_i^* \\ &= -\zeta_i^*\left(1 - e^{-C_i\theta}\right) + \zeta_p\left(1 - e^{-C_p\theta}\right)\end{aligned} \tag{5}$$

To understand and visualise equation (5), we plot $\mathbf{\Delta}\zeta^*$ vs. θ for three distinct cases, i.e. proteins carrying a net positive charge ($\zeta_p>0$), nearly neutral ($\zeta_p \sim 0$) and negative charge ($\zeta_p<0$). Fig. 1(a) considers the case of neutral proteins. We define the normalized radius $a_r = a/\lambda$. For calculating θ, we consider the attached proteins to occupy an area equivalent to that of a disc of radius a. The figure shows a plot of $\mathbf{\Delta}\zeta^*$

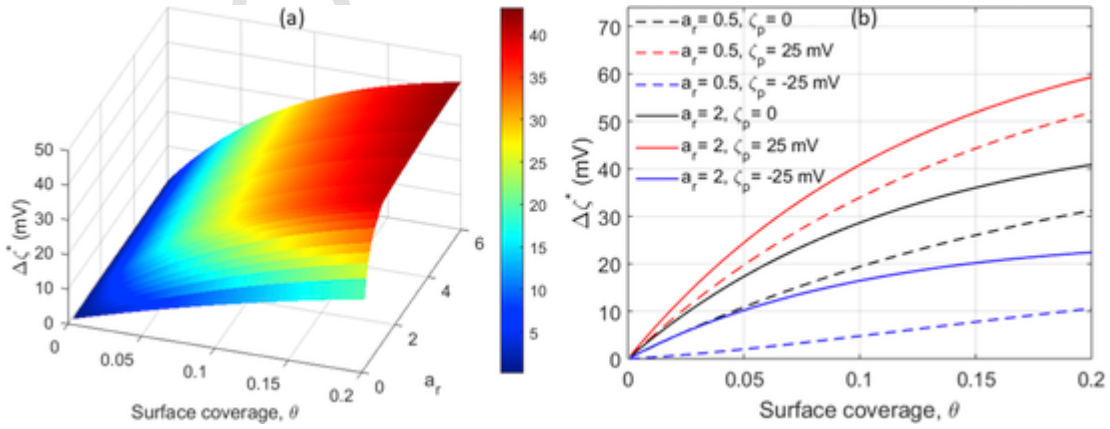

Fig. 1. (a) Sensor response to neutral proteins shown as a 3D graph of $\Delta\zeta^*$ vs a_r and θ. The sensor response increases with the relative size (a_r), and starts to saturate at $a_r>1$. (b) The influence of charge on the signal and sensitivity for a_r = 0.5 and 2 respectively when ζ_p = 25, 0 and −25 mV. In all these cases, ζ_i^* = −50 mV and C_i and C_p values are taken from (Adamczyk et al., 2010).

vs a_r and θ. Clearly, for small θ and a_r, the $\Delta\zeta^*$ increases with both of them and then gradually saturates in both cases. In terms of the slope of $\Delta\zeta^*$ vs a_r plot (Fig. 1(a)), the rate of increase in $\Delta\zeta^*$ as a function of particle size decreases with increasing particle size and gradually becomes negligible as a_r becomes larger than the Debye screening length $(a_r>1)$. This highlights that size effects are significant only as long as it is of the order of λ, beyond which, further increase in protein size no longer influences the streaming current at the interface. However, proteins also carry electric charges arising due to their various amino acids that can get ionized in a polar solvent (Janson and Rydén, 1998). The magnitude and sign of these charges depends on the pH of the buffer. Both of these factors ultimately decide the value of ζ_p for the protein. In order to investigate the influence of ζ_p, we simulated the influence of particles with three different values of ζ_p (-25, 0 and 25 mV) and binding to a negatively charged surface ($\zeta_i = -50$ mV), as shown in Fig. 1(b). The selection of the above-mentioned values of ζ_i^* and ζ_p allows us to use the values of C_i and C_p which are previously determined (Adamczyk et al., 2010). We also considered two different protein sizes, $a_r = 0.5$ and 2, in order to evaluate the combined effect arising from both the sizes and charges. As seen in Fig. 1(b), the sensor response and sensitivity is the highest when the proteins carry the opposite charges ($\zeta_p = 25$ mV) relative to the initial charge on the surface and lowest in the complementary case ($\zeta_p = -25$ mV). In addition, the simulation also predicts a stronger signal for larger molecules irrespective of their charge type. It is important to note that the channel dimensions are large enough so that solvent polarization (Das et al., 2012) and steric hindrance (Garai and Chakraborty, 2010) effects are insignificant for our case.

In order to experimentally evaluate the simulated dependence of the molecular size and zeta potential on the sensor response, a series of measurements were done at physiological pH with a set of well-characterized proteins. As model proteins, four different affibodies, that were derived from the same parental protein by exchange of distinct amino acids were used in monomeric and/or dimeric form to allow the investigation of seven proteins of different sizes. Due to the different amino acid composition of each affibody protein, their zeta potential varies a lot allowing for the assessment of this important factor (Table 1). A covalent coupling strategy was used for the surface attachment of the proteins in order to ensure irreversible coupling to the surface for all proteins. In a typical real-time response, the arrival of the sample plug at the capillary channel induces a strong and immediate drop of ζ^* (Fig. 2(a)) followed by a slow increase during the sample injection. A similar behaviour is also recorded when the sample plug is replaced by the buffer plug. Such a behaviour is common in biosensing and is usually attributed to bulk composition effects (O'Brien II et al., 1999). A net increase in ζ^* can be seen between the two buffer plugs representing the signal, $\Delta\zeta^*$. Arrows mark the start and end of the injection. Unless mentioned otherwise, in all experiments the initial baseline of the surface had a ζ_i value of -34 ± 2 mV and either increased or decreased from this value upon sample injection.

The signals for all the affibody proteins have been summarized in Fig. 2(b) as bar plot where the height of the bar represents the $\Delta\zeta^*$ for the corresponding measurement. Each result has been control-subtracted and presented as an average, along with standard deviation (SD) over at least three measurements. For simplicity, we grouped the results in three categories; (i) nearly charge neutral affibodies ($\zeta_p \sim 0$) under our experimental conditions (set N, monomeric affibody N1 and dimeric affibody N2), (ii) those carrying opposite charge ($\zeta_p>0$) with respect to the initial zeta potential of the surface (set O, dimeric affibody O2) and (iii) those carrying the same charge type ($\zeta_p<0$) as the surface (set S, affibodies S1A, S1B, S2A and S2B). We would like to emphasize here that for accurate experimental evaluation of the size and the charge effects, one would ideally need a set of similar particles either differing in their sizes or ζ_p only, keeping the other parameter identical. However, it is difficult to obtain such a set of samples and therefore, the experimental validation was done with proteins that qualitatively resemble the aforementioned ideal conditions.

4.1. Protein set N: nearly neutral proteins with different sizes

Fig. 2(b) shows the signal of two affibodies, N1 and N2, where the dimeric version is 1.5-fold larger than the monomeric form in terms of its hydrodynamic radius. N1 and N2 are almost neutral with ζ_p about 0.2 and 0.3 mV, respectively (see Table 1) in 0.1 ×PBS. It can be seen that the average signal from the N2 is about five times larger than that obtained from the N1. Moreover, both N1 and N2 induce an increase in ζ^* i.e., $\Delta\zeta^*>0$, as predicted from the theory (Fig. 1(b)). The shaded region on both sides of the baseline refers to the noise floor (which is $3 \times SD = 0.1\ mV$).

4.2. Protein set O: carrying opposite charge as compared to the surface

To understand the influence of a positively charged protein bound to a negatively charged surface, we compare the signal from O2 against the nearly neutral N2. Each O2 molecule carries a net positive charge with ζ_p about 2.7 mV while having a slightly smaller size than N2. O2 induces a signal of ~2.0 mV, which is almost twice the signal induced by N2. Indeed, the O2

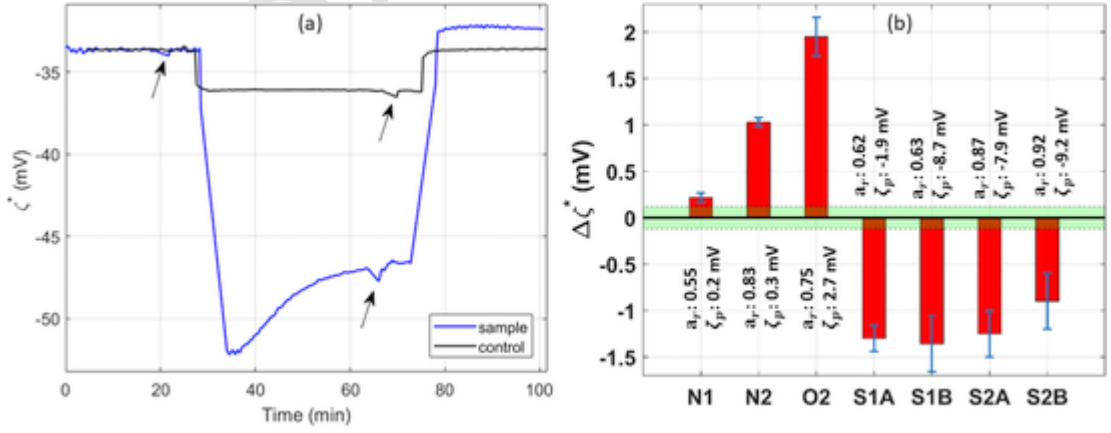

Fig. 2. (a) A real-time signal of the binding of affibody N2, along with its control measurement. The arrows indicate the start and end of injection. The difference between the initial and final baseline constitutes the signal $\Delta\zeta^*$. (b) Bar plots comparing the sensor signal $\Delta\zeta^*$ for neutral affibodies N1 and N2; and positively charged O2 and negatively charged affibodies S1A, S1B, S2A and S2B. The values of a_r and ζ_p of each affibody is mentioned adjacent to its corresponding bar plot. The shaded area indicates the noise floor of 0.1 mV.

affibody shows the strongest signal among all the dimers that

we tested. Hence, these results too are consistent with the theoretical predictions presented in Fig. 1.

4.3. Protein set S: same type of charges as the surface and different sizes

In Fig. 2(b), the signals arising from S1A, S1B, S2A and S2B are also compared. In this particular case, all the affibodies carry the same type of charge as the capillary surface (negative) with ζ_p of −1.9, −7.5, −8.7 and −9.2 mV respectively. It can be seen that unlike the previous cases, $\Delta\zeta^*<0$ for all the affibodies, i.e. $\left|\zeta_f^*\right| > \left|\zeta_i^*\right|$. Interestingly, the response from the dimer S2A is not very different from that of the monomers S1A and S1B, despite having large differences in their ζ_p and the particle size. Moreover, in our repeated measurements, the largest and most negative protein type (S2B) in this group actually showed the weakest response among all the proteins in this category. Both of these observations are clear deviations from the theoretically expected behaviour (Fig. 1(b)) where a molecule with larger size parameter is expected to induce stronger response irrespective of their charge type and the net signal is expected to be positive even for negatively charged affibodies.

Even though studies at physiological pH are of actual relevance for biosensing, in order to gain further insight into the influence of molecular charge on the signal, we performed a set of measurements with N1 and N2, however, with different pH of the buffer. This allows to vary the net charge of the molecules while keeping their size identical. For this purpose, pH of PBS buffers were adjusted to pH 6.4, and 8.4 in two separate experiments. This range of the pH was selected to be able to modulate the ζ_p of the molecules from positive to negative values. The modified ζ_p of the molecules in each of the buffers were measured using ELS, and are presented in Fig. 3(a). It should be noted that the zeta potential of the surface (ζ_i^*) also changes with the pH of the buffer and is expected to influence the sensor response (equation (5)). Therefore the ζ_i^* of the surface at these pH's was recorded (Fig. 3(b)). It can be seen that the ζ_i^* remains sufficiently negative and linearly changes from −31.5 to −36 mV as the pH changes from 6.4 to 8.4. Furthermore, in order to maintain identical conditions for binding, the molecules were dispersed and injected at pH 7.4, and only the baselines before and after the sample injections were taken at the other pH. The resulting signal $\Delta\zeta^*$ for these pH dependent measurements are shown in Fig. 3. As the ζ_p of the monomer changes from 0.7 to −0.8 mV, the sign and the strength of the signal also changes reflecting the influence of the electric charges (Fig. 3(c)). A similar trend is also visible for the dimer (Fig. 3 (d)). For positive charges, the binding of both the monomer and the dimer leads to $\Delta\zeta^*>0$. However, the dimeric affibody induces a much larger signal compared to the monomer. As the ζ_p approaches zero, the signal remains positive for both affibodies, but has a smaller value as compared to when ζ_p is positive. Finally, as the ζ_p becomes negative, the signal for the affibodies is inverted. It should be noted that, although the ζ_p is varied by approximately the same amount to either side of the neutral condition, the monomeric and the dimeric affibodies show a very different behaviour. While the monomeric affibody shows a very similar signal strength for both the positive and the negative ζ_p, the dimeric affibody shows almost a six times larger signal for the positive ζ_p compared to the negative ζ_p. This behaviour is clearly not in agreement with our initial theoretical analysis (Fig. 1). Further discussion about this apparent discrepancy and any possible influ-

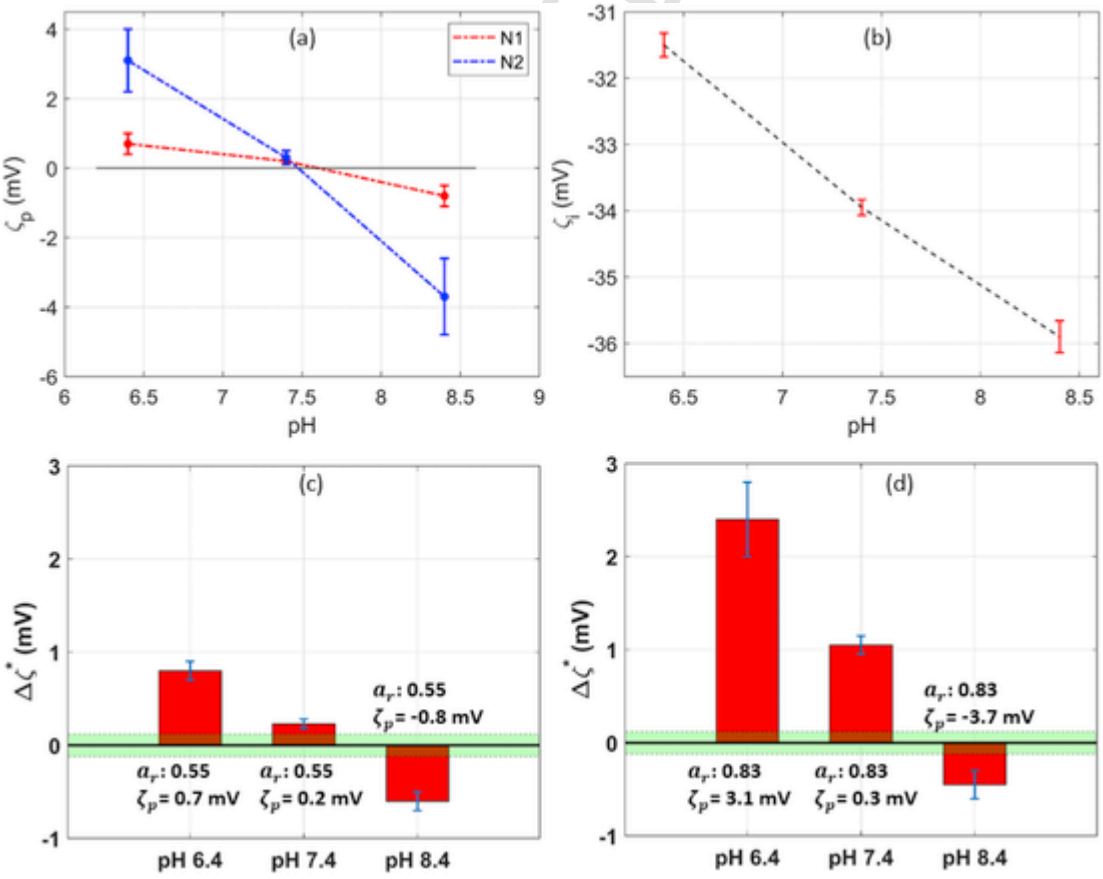

Fig. 3. (a) Variation of ζ_p of affibodies N1 and N2 with the error bars indicating the standard deviation. (b) Variation ζ_i^* with pH for the pH dependent measurements, with the error bars indicating the noise floor in the baselines. While the ζ_p inverts in sign for this pH range, ζ_i remains sufficiently negative. The next two panels show the pH dependent study of the binding signal ($\Delta\zeta^*$) in the case of the affibodies (c) N1 and (d) N2. The bar plots are obtained as mean from two measurements and presented along with the SD, after control subtraction. The values of a_r and ζ_p of each affibody are mentioned adjacent to its bar plot. The shaded area indicates the noise floor of 0.1 mV.

ence arising from the changes in ζ_i^*, induced by the changes in the buffer pH, has been provided in the subsequent section.

Having demonstrated the influence of molecular size and ζ_p on the sensor response, we investigated the extent of such influence from molecules which have very large differences in their sizes and ζ_p. For this purpose, we selected three proteins: the affibody O2, the antibody CET, and the complement component C1Q. Among the selected molecules, C1Q has the largest size and charge parameters ($\mathbf{a_r} = 2.2$; $\zeta_p = 19.6$ **mV**), followed by CET ($\mathbf{a_r} = 1.6$; $\zeta_p = 1.5$ **mV**). The dimeric affibody O2 has the smallest size and intermediate charge parameter among them ($\mathbf{a_r} = 0.8$; $\zeta_p = 2.7$ **mV**). The concentration dependent response from the sensor is presented in Fig. 4 as semi-logarithmic plots. For comparison, we define the term sensitivity (S_i) of the device as the minimum concentration of an injected molecule at which the sensor response is equal to the noise floor (3 × SD of noise calculated from the initial baseline). This concentration was estimated from an exponential fit of the signal vs. concentration curve (Fig. 4). As expected C1Q shows the strongest response among them followed by CET and O2. The value of S_i is 3.75 nM for CET while for C1Q, there is a 14-fold improvement in the S_i, which becomes 0.26 nM. In comparison to O2 (S_i = 69.24 nM), C1Q shows a 266-fold improvement in sensitivity. It is important to point out here that the sensitivity is not used in the conventional sense as used in the case of specific and reversible interaction achieved through affinity reagents. Instead, we are using it merely for quantitative comparison of the sensor for a case of random sequential adsorption carried out for a time-limited injection (40 min).

5. Discussion

As mentioned before, electrokinetic principles have been very useful to study protein-covered surfaces and several investigations involving the study of protein adsorption kinetics have been reported (Alkan et al., 2006). A major issue with the method stems from the fact that the surface adsorption of proteins influences both the local electrostatics and hydrodynamics, resulting in a strong dependence of the electrokinetic signal on the size and the charge parameters of the proteins. A positive consequence of this aspect is that a molecule can be detected irrespective of its electrical charge. However, the dependence on size and charge of a molecule means that the sensitivity of the method may vary over a very wide range. Recent reports on biomolecule sensing using electrokinetic principles, which reveals LOD varying from

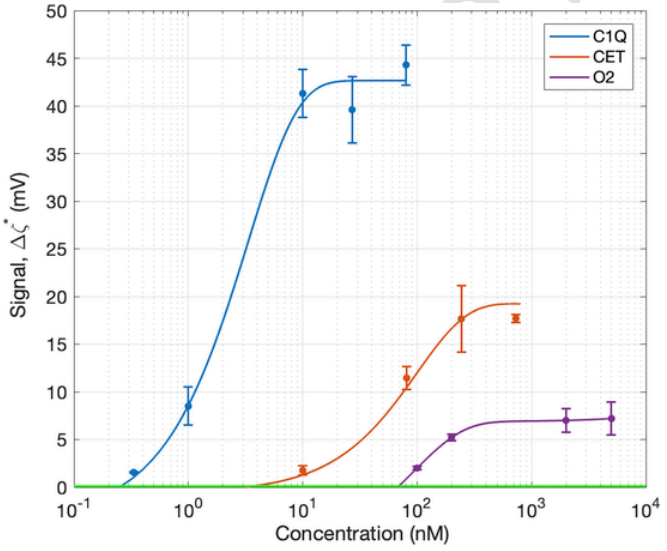

Fig. 4. Sensor response for C1Q, CET and O2 for various concentrations. C1Q, being larger in both size and bearing higher positive charge, shows stronger response and sensitivity in comparison to CET and O2. The values of S_i for C1Q, CET and O2 are 0.26 nM, 3.75 nM and 69.24 nM respectively.

e.g. 10 nM (Li et al., 2018) to 460 fM (Cavallaro et al., 2019), is a clear testament of this behaviour. Aiming to understand such a large variation in the sensitivity, we utilized here a recently developed theoretical model to simulate the sensor response as a function of the surface coverage for three different classes of proteins in terms of their size and charges (Fig. 1). The experimental investigations of different cases (Fig. 2(b)) are further discussed here.

5.1. Case I: Nearly neutral molecules with different sizes

In the case of charge neutral molecules, the signal and hence the sensitivity is expected to improve with the protein sizes (Fig. 1(a)). In this case, $|\zeta_f^*| < |\zeta_i^*|$, leading to a positive net signal i.e. $\Delta\zeta^* > 0$. This is because the attached proteins on the surface provide additional impedance to the flow of ions (Zembala and Adamczyk, 2000). This behaviour is also clearly evident in the results for N1 and N2 (Fig. 2(b)). The attached proteins may also influence the local electric field of the charges on the capillary surface due to the difference in permittivity between the electrolyte and the adsorbed protein molecules. It may be noted here that the dimeric affibody which is just ~27% larger in terms of its hydrodynamic radius, induces a ~5 times stronger signal. A small difference in their ζ_p may also partly contribute to the observed differences in their signal. A similar size dependence was also reported for colloidal particles and this originates as a consequence of damping of convection currents of ions in the vicinity of adsorbed molecules (Zembala and Adamczyk, 2000). This leads to a decrease in the measured streaming current and hence $\Delta\zeta^* > 0$. The effect, however, is expected to saturate as the protein size becomes large relative to the Debye screening length (Fig. 1(a)).

5.2. Case II: Effect of molecular charges: molecules carrying opposite charges than the surface

The binding of a positively charged molecule on a negatively charged surface is expected to induce a larger signal as compared to a neutral molecule of same size (Fig. 1(b)). This is indeed the case (Fig. 2(b)), where the nearly neutral dimer, N2 is compared with the positively charged dimer O2. Even though O2 is slightly smaller than N2 in terms of a_r, it exhibits around twice as much the signal. Binding of molecules carrying opposite charges than the surface partly neutralizes the electric field of the surface charges and therefore reduces the streaming current. With larger ζ_p, a stronger effect is expected. A similar effect can be seen in the pH dependent studies (Fig. 3). As the ζ_p increases from 0.2 to 0.7 mV for the investigated monomer and from 0.3 to 3.1 mV in the case of the dimer, the $\Delta\zeta^*$ increases in both the cases. Indeed, for more accurate interpretation of the pH dependent study, one should take into account the changes in ζ_i^* as reflected in equation (6).

$$\Delta\zeta^* = -\zeta_i^* \left(1 - e^{-C_i\theta}\right) + \zeta_p \left(1 - e^{-C_p\theta}\right) \quad (6)$$

Clearly, both ζ_i^* and ζ_p influence the signal arising from the adsorption of molecules to the surface and the change of buffer pH also changes ζ_i^* (Fig. 3(b)). However, their relative influence is determined by the values of C_i and C_p, as seen in equation (6). Although the exact values of these parameters for the proteins used in this study are not known, their general dependences on the parameter a/λ have been calculated for several cases (Adamczyk et al., 2010), which clearly suggest C_p to be significantly larger than C_i for $a/\lambda < 1$. In addition, the initial roughness of the surface may also play a significant role here, further reducing the influence of C_i. It is known that the streaming current is expected to decrease with increasing surface roughness (Adamczyk et al., 2010). Practically, the surface roughness has a similar effect on the signal as that of protein deposition on a smooth surface with the condition that $\zeta_p = \zeta_i^*$. As explained earlier, both of these condi-

tions result in a damping of convection currents from ions close to the surface. However, when molecules with size comparable to the surface roughness are adsorbed, the resultant effect is expected to be weaker diminishing the influence of C_i further. To get a further insight, a simulated plot for proteins matching the size of our monomers and dimers is presented in Fig. 5(a). The figure shows the extent of influence on $\Delta\zeta^*$ expected as a result of changes in ζ_i^*, arising as a consequence of pH change. However, to take into account the influence of roughness, the values of C_i for monomers and dimers, respectively, were assumed to be 0.49 and 1.70, which are 10 times and 5 times smaller compared to theoretical values of C_i obtained from numerical simulations (Adamczyk et al., 2010) for the corresponding values of a_r. It can be seen that as ζ_i^* changes from −36 to −31.5 mV, the overall signal changes by 0.18 mV and 0.38 mV for the monomer and the dimer respectively. In comparison, the changes in the experimentally determined $\Delta\zeta^*$ for N1 and N2 are 1.4 and 2.9 mV, respectively, as seen in Fig. 3. Clearly the effect is ~6 times stronger indicating only a weak influence from the changes in the ζ_i^* as a result of pH change.

5.3. Case III: Effect of molecular charges: molecules carrying same type of charges as the surface

The case of negatively charged molecules adsorbed on a negatively charged surface (Fig. 2(b)), however, shows a clear disagreement with the initially simulated results (Fig. 1(b)). According to our earlier simulation, the signal arising from the adsorption follows the same trend as that of the positively charged molecules but should be relatively weaker. In contrast, the experimental results for the negatively charged affibodies show inversion of signal (Fig. 2(b)), i.e. $\Delta\zeta^*<0$ and also the differences in signal between the monomers S1A, S1B, and the dimer S2A are negligible. The larger ζ_p of the S2A (−7.5 mV) compared to S1A (−1.9 mV) also does not seem to play any major role in this case. In order to investigate this discrepancy, we first simulated the variation of the signal, $\Delta\zeta^*$ with the parameter C_i for the negatively charged case (see figure S3). According to the Adamczyk model (Adamczyk et al., 2010), the simulated values of C_i attain a saturation value of 10.21 when plotted against a_r. So, we varied C_i from 0 to 10.21 and plotted $\Delta\zeta^*$ as a function of C_i. We found that the sign of $\Delta\zeta^*$ indeed inverts below a certain value of C_i for $\zeta_p< 0$. In contrast, the sign remains the same for $\zeta_p>0$ for this range of C_i. Fig. 5(b) shows a simulated response curve ($\Delta\zeta^*$ vs. θ) for the same set of molecular parameters as presented in Fig. 1(b), however, for values of C_i which are now smaller than the ones extracted from simulations in (Adamczyk et al., 2010). In this particular case, we set the values of C_i to be 10 times and 5 times lower for the smaller $(a_r = 0.5)$ and the larger $(a_r = 2)$ particle, respectively. Clearly, the trends now show consistency with the experimental observations. It can be seen that the overall response in all cases is lower than the previously calculated values. The relative behaviour of the oppositely charged particles and charge neutral particles remains similar including the signal dependence on the particle sizes. However, for the case of negatively charged particles, the response is significantly different from the earlier case. Not only is the direction of the response opposite to the one predicted previously, but also the smaller particle shows a larger response. A similar effect can be observed upon comparing the signal from the affibodies S1B and S2B (see Fig. 2(b)). In this case, the larger affibody S2B induces a weaker response, as predicted by the updated simulations. A lower value of C_i was also used to explain the experimental results in another study involving nanoparticles (Michelmore and Hayes, 2000). We believe this is due to the fact that the functionalised surface has some roughness which is comparable to the radius of the attached proteins. It is expected to be more significant for the smaller proteins than the larger ones.

As can be seen from the sensitivity estimation (Fig. 4), there is a 266-fold disparity in the values for O2 and C1Q. Moreover, the sensitivity can be modulated by controlling the charge of the proteins and their sign in relation to the surface. As we demonstrated in the pH dependent studies of the affibodies N1 and N2, the same protein can induce different response depending on the charge it bears, as well as the sign of charge in relation to the sensor surface. Hence, by varying this charge either by modifying the pH or the charge on the sensor surface (either by choosing suitable materials or chemical treatments), the sensitivity can be significantly improved. Similarly, improved response can be achieved by increasing the normalized radius of the protein or through changing the ionic strength of the measurement buffer to reduce λ. These arguments can be extended to the case of specific bio-detection. The vast majority of literature refers to a general value of the limit of detection (LOD) when referring to biosensors, but as our results show, this would depend on the molecule being studied. Moreover, since the LOD of the sensor is a major limiting factor for the detection of low abundance analytes, the study presented here can guide the selection of experimental parameters for an improved sensitivity. Apart from detection of proteins, these results can also be used for studying DNA hybridization reactions in microchannels (Das et al., 2006; Das and Chakraborty, 2007).

6. Conclusions

In summary, we demonstrate that the sensitivity of electrokinetic sensor relying on streaming current measurements is strongly influenced by the size and zeta potential of the target molecule. The sen-

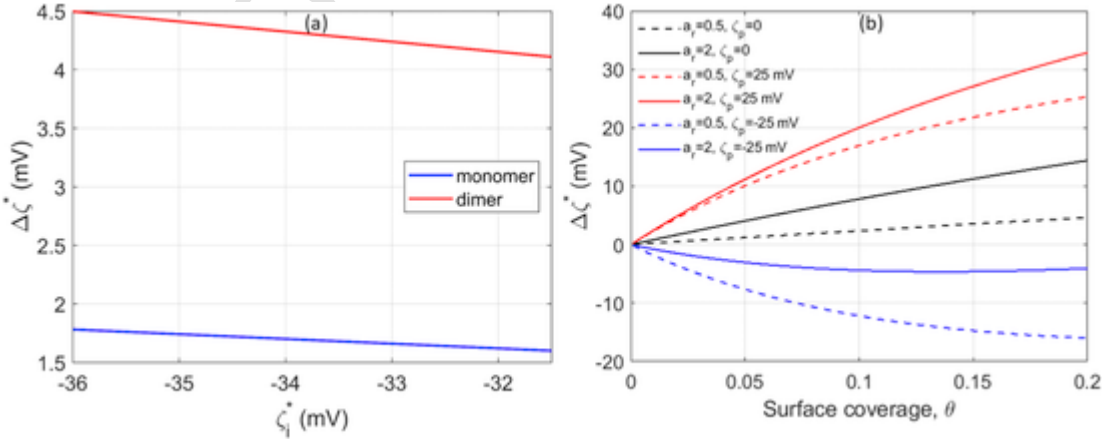

Fig. 5. (a) Influence of the baseline zeta potential of the surface (ζ_i^*) on the signal ($\Delta\zeta^*$) for N1 and N2. The ζ_i^* indeed has a very small contribution to the overall signal in this case, which means that the ζ_p of the proteins have a dominant influence over the signal. (b) Variation of $\Delta\zeta^*$ with θ for $a_r = 0.5$ and 2 and $\zeta_p = 25$, 0 and −25 mV but with smaller values of C_i than those mentioned in Fig.(Adamczyk et al., 2010). The behaviour of the proteins is markedly different from Fig. 1 for $\zeta_p = -25$ mV.

sor characteristic is analysed both theoretically, by using an established model, and experimentally by using a set of well-characterized proteins having molecular size and zeta potential (at pH 7.4) in the range 9–460 kDa and −9.2 to 19.6 mV respectively. The results, in qualitative agreement with the theoretical predictions, show that the sensor response increases with molecular size and zeta potential when molecules carrying opposite charge type than the surface is conjugated to the surface. Similar size dependence is also observed for molecules carrying no net charges. However, the influence of the molecular size gradually saturates as the diameter exceeds the Debye screening length of the electrolyte. In contrast and in apparent disagreement with the theory, the conjugation of molecules carrying the same charge type as the surface show little or no dependence on molecular size and their zeta potential, except that the sign of the signal inverts. The behaviour can however, be explained within the same theoretical basis but considering stronger influence from the surface roughness. The study further demonstrates that the sensitivity of such a sensor may vary over several orders of magnitude as a result of the difference in the molecular sizes and their zeta potential. The results presented here can be utilized to analyse the sensor response for various molecules as well as to optimize the experimental parameters for improved sensitivity.

CRediT authorship contribution statement

Siddharth Sourabh Sahu: Validation, Writing - original draft. **Christiane Stiller:** Writing - original draft, Writing - review & editing. **Amelie Eriksson Karlström:** Project administration, Funding acquisition. **Jan Linnros:** Project administration, Writing - review & editing. **Apurba Dev:** Conceptualization, Project administration, Funding acquisition, Writing - original draft, Writing - review & editing.

Declaration of competing interest

The authors declare that they have no known competing financial interests or personal relationships that could have appeared to influence the work reported in this paper.

Acknowledgments

The authors acknowledge financial support by the Erling Persson foundation. The authors AD and SSS also acknowledge the support from the Swedish Research Council (grant no. 2016-05051). We are thankful to RISE Acreo for supporting us with microcapillaries.

Appendix A. Supplementary data

Supplementary data related to this article can be found at https://doi.org/10.1016/j.bios.2020.112005.

References

Adamczyk, Z., Sadlej, K., Wajnryb, E., Nattich, M., Ekiel-Jezewska, M.L., Bławzdziewicz, J., 2010. Adv. Colloid Interface Sci. 153, 1–29. doi:10.1016/j.cis.2009.09.004.
Alkan, M., Demirbaş, Ö., Doğan, M., Arslan, O., 2006. Microporous Mesoporous Mater. 96, 331–340. doi:10.1016/j.micromeso.2006.07.007.
Cavallaro, S., Horak, J., Hååg, P., Gupta, D., Stiller, C., Sahu, S.S., Görgens, A., Gatty, H.K., Viktorsson, K., El-Andaloussi, S., Lewensohn, R., Eriksson Karlström, A., Linnros, J., Dev, A., 2019. ACS Sens. 9b00418. doi:10.1021/acssensors.9b00418.
Chen, X., Guo, Z., Yang, G.-M., Li, J., Li, M.-Q., Liu, J.-H., Huang, X.-J., 2010. Mater. Today 13, 28–41. doi:10.1016/S1369-7021(10)70201-7.
Chen, Y., Ren, R., Pu, H., Guo, X., Chang, J., Zhou, G., Mao, S., Kron, M., Chen, J., 2017. Sci. Rep. 7, 10974. doi:10.1038/s41598-017-11387-7.
Das, S., Chakraborty, S., 2007. AIChE J. 53, 1086–1099. doi:10.1002/aic.11144.
Das, S., Chakraborty, S., Mitra, S.K., 2012. Phys. Rev. E - Stat. Nonlinear Soft Matter Phys. 85. doi:10.1103/PhysRevE.85.051508.
Das, S., Das, T., Chakraborty, S., 2006. Sens. Actuators B Chem. 114, 957–963. doi:10.1016/j.snb.2005.08.012.
Delgado, A.V., González-Caballero, F., Hunter, R.J., Koopal, L.K., Lyklema, J., 2007. J. Colloid Interface Sci. 309, 194–224. doi:10.1016/J.JCIS.2006.12.075.
Dev, A., Horak, J., Kaiser, A., Yuan, X., Perols, A., Björk, P., Karlström, A.E., Kleimann, P., Linnros, J., 2016. Biosens. Bioelectron. 82, 55–63. doi:10.1016/j.bios.2016.03.060.
Downs, A.M., McCallum, C., Pennathur, S., 2019. Electrophoresis 40, 792–798. doi:10.1002/elps.201800356.
Erickson, H.P., 2009. Biol. Proced. Online 11, 32–51. doi:10.1007/s12575-009-9008-x.
Garai, A., Chakraborty, S., 2010. Electrophoresis 31, 843–849. doi:10.1002/elps.200900676.
Hanaor, D.A.H., Ghadiri, M., Chrzanowski, W., Gan, Y., 2014. Langmuir 30, 15143–15152. doi:10.1021/la503581e.
Hayes, R.A., 1999. Colloid. Surf. Physicochem. Eng. Asp. 146, 89–94. doi:10.1016/S0927-7757(98)00864-4.
Hayes, R.A., Böhmer, M.R., Fokkink, L.G.J., 1999. Langmuir 15, 2865–2870. doi:10.1021/la980668f.
Horak, J., Jansson, R., Dev, A., Nilebäck, L., Behnam, K., Linnros, J., Hedhammar, M., Karlström, A.E., 2018. Adv. Funct. Mater. 28. doi:10.1002/adfm.201800206.
Janson, J.-C., Rydén, L., 1998. Protein Purification: Principles, High Resolution Methods and Applications. second ed. Wiley-Blackwell.
Joly, L., Ybert, C., Trizac, E., Bocquet, L., 2004. Hydrodynamics within the Electric Double Layer on Slipping Surfaces.
Levine, S., Marriott, J., Neale, G., Epstein, N., 1975. J. Colloid Interface Sci. 52, 136–149. doi:10.1016/0021-9797(75)90310-0.
Li, Y., Lai, S.N., Zheng, B., 2018. Sens. Actuators B Chem. 259, 871–877. doi:10.1016/J.SNB.2017.12.130.
Löfblom, J., Feldwisch, J., Tolmachev, V., Carlsson, J., Ståhl, S., Frejd, F.Y., 2010. FEBS Lett. 584, 2670–2680. doi:10.1016/j.febslet.2010.04.014.
Michelmore, A.P., Hayes, R.A., 2000. PhysChemComm 3. doi:10.1039/b001277g.
O'Brien, M.J., II, Brueck, S.R.J., Perez-Luna, V.H., Tender, L.M., Lopez, G.P., 1999. Biosens. Bioelectron. 14, 145–154. 1998. doi:10.1016/S0956-5663(98)00121-3.
Sadlej, K., Wajnryb, E., Bawzdziewicz, J., Ekiel-Jeewska, M.L., Adamczyk, Z., 2009. J. Chem. Phys. 130. doi:10.1063/1.3103545.
Tashiro, M., Tejero, R., Zimmerman, D.E., Celda, B., Nilsson, B., Montelione, G.T., 1997. J. Mol. Biol. 272, 573–590. doi:10.1006/jmbi.1997.1265.
Zembala, M., Adamczyk, Z., 2000. Langmuir 16, 1593–1601. doi:10.1021/la9905970.
Zembala, M., Adamczyk, Z., Warszyński, P., 2003. Colloid. Surf. Physicochem. Eng. Asp. 222, 329–339. doi:10.1016/S0927-7757(03)00253-X.
Zembala, M., Adamczyk, Z., Warszyski, P., 2001. Colloid. Surf. Physicochem. Eng. Asp. 195, 3–15. doi:10.1016/S0927-7757(01)00825-1.